ACS APPLIED BIO MATERIALS Cite This: ACS Appl. Bio Mater. 2018, 1, 59−69 Article www.acsabm.org

Optoelectronic Properties of Diamondoid-DNA Complexes

Chandra Shekar Sarap,[†] Pouya Partovi-Azar,[*,‡] and Maria Fyta[†]

[†]Institute for Computational Physics, Universität Stuttgart, Allmandring 3, 70569 Stuttgart, Germany

[‡]Institute of Chemistry, Martin Luther University Halle-Wittenberg, Von-Danckelmann-Platz 4, 06120 Halle (Saale), Germany

ABSTRACT: DNA sensing with engineered nanomaterials can bestow a new platform for single nucleotide identification and sequencing. Nevertheless, understanding the relevant nano-bio interfaces can provide a wealth of information on structures, energetics, and dynamics with a great potential in molecular nanotechnology. Herein, we explore the sensitivity of DNA units, the nucleotides, with a tiny probe, the diamond-like structures known as diamondoids. The probe diamondoid and the target nucleotides interact via hydrogen bonding, forming nano-bio complexes. The binding strengths for these complexes lie between the physisorption and chemisorption, allowing a suitable probe to sense the DNA nucleotides. Besides electronic properties, herein we investigate the optical properties of the nucleotides interacting with a functional diamondoid for the first time by assessing the absorption spectra and the charge dynamics within these complexes. The relative arrangements and bonding characteristics of the diamondoid with the nucleotides strongly influence these properties. Interestingly, we observe charge transfer oscillations between the diamondoid and few nucleotides, while one-way transfer or no charge transfer is observed in other cases. Our results provide a deeper understanding of the inherent electron dynamics of these complexes and can be utilized to design functionalized devices for optical detection. The presented approach can be proven essential in determining the properties of molecular complexes targeted for novel applications in sensing and nanoelectronics.

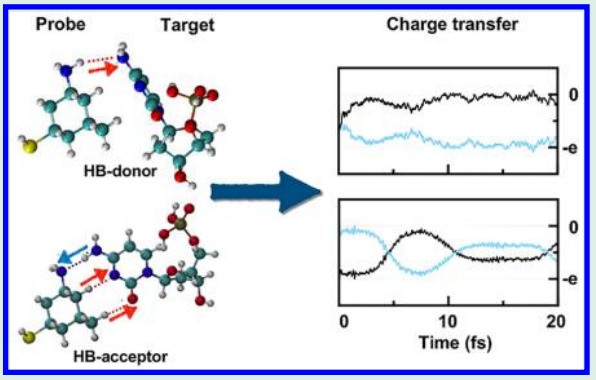

KEYWORDS: *diamondoids, nucleotides, absorption spectra, charge dynamics, TDDFT*

INTRODUCTION

The interplay of nanostructured materials with biomolecules is essential in describing their biocompatibility that outsources to give various applications in biosensors, drug delivery, and molecular recognition.[1,2] Carbon-based materials such as fullerenes, carbon nanotubes, graphene and its derivatives, etc. have unique and often tunable optical, electronic, and mechanical properties that have diverse applications in self-assembly, catalysis, hydrogen production, energy storage, and in photonic devices.[3−7] These nanostructures can be used in effective sensing devices to detect various biomolecules.[8−11] Numerous biologically related experiments and theoretical studies have been carried out on carbon-based materials and have proven to be an excellent platforms for DNA hybridization and sequencing.[11−14]

Carbon-based nanostructures with a high potential for applications are the diamondoids.[15,16] These are nanometer-sized hydrogen-terminated diamond-like cages with sp^3 hybridization of carbon complementing the sp^2 carbon nanomaterials such as graphene, CNT, and fullerenes. Diamondoids exist in various sizes, adamantane being the smallest with a single diamond cage. It is followed by diamantane with an additional diamond crystal cage, triamantane with an extra three fused cages, etc. Small diamondoids have been isolated primarily from crude oil[16] and can be chemically synthesized and modified,[17,18] as also predicted through quantum mechanical simulations.[19] Due to the wide range of sizes and derivatives, tuning of their properties can quite easily be achieved.[20−22] Accordingly, these molecules have recently gained a lot of interest owing to their high thermal stability, superior chemical resistance, and negative electron affinity. These properties suggest their utilization in a plethora of applications ranging from electron emitting devices and surface emission to sensing, electrochemistry, drug delivery, and microelectronics.[15,16,23−25] Moreover, diamondoid derivatives with specific functional groups have a wide range of applications in pharmaceuticals, nanomaterials, and optical devices.[18,26] Representative diamondoid derivatives have also shown excellent biocompatibility, suggesting their synthesis and functionalization for drug development.[27] Adamantane-based drugs have already been used as inhibitors for the reproduction of viruses by forming the hydrogen bond with the histidine residue in the transmembrane domain protein of viruses.[28] These derivatives have also been utilized as chemotherapeutics against many infectious diseases including herpes simplex, hepatitis C, HIV, and malaria.[18]

Recently, we have explored the possibility of using diamondoid derivatives as probes to distinguish DNA nucleotides in their natural and mutated form.[29] Nucleotides are the building blocks of DNA molecules and understanding the structures and energetics of the nucleotides interaction with

Received: April 19, 2018
Accepted: May 30, 2018
Published: May 30, 2018

DOI: 10.1021/acsabm.8b00011
ACS Appl. Bio Mater. 2018, 1, 59−69

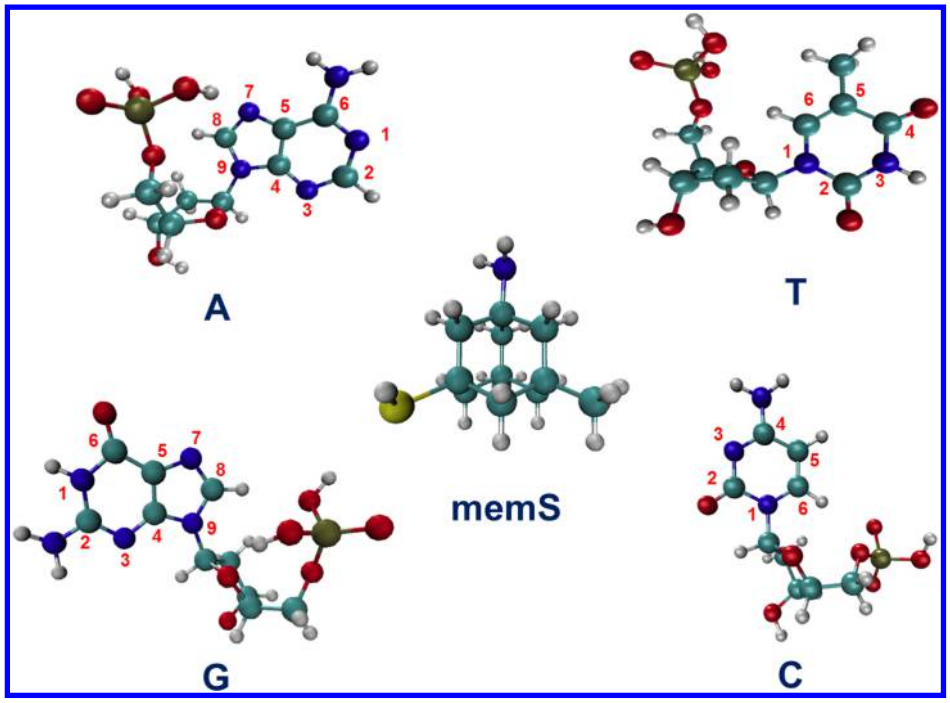

Figure 1. Optimized gas-phase geometries of various isolated nucleotides, A (2′-deoxyadenosine 5′-monophosphate, $C_{10}H_{14}N_5O_6P$), T (2′-deoxythymidine 5′-monophophate, $C_{10}H_{14}N_2O_8P$), G (2′-deoxyguanosine 5′-monophosphate, $C_{10}H_{14}N_5O_7P$), C (2′-deoxycytidine 5′-monophosphate, $C_9H_{14}N_3O_7P$), and the functionalized diamondoid, memS (mementine-thiol, $C_{12}H_{21}NS$). The hydrogen, carbon, nitrogen, oxygen, phosphorus, and thiol atoms are colored in white, cyan, blue, red, tan, and yellow, respectively. The same color coding will be used throughout.

carbon-based nanomaterials can shed light onto the phenomena occurring at the nano-bio interfaces. The driving forces behind the interaction of these nucleotides with the carbon-based structures are the electrostatic, $\pi-\pi$ stacking, hydrogen bonding, and long-range dispersion interactions. Earlier, strong nucleotide-specific features are found in the electronic transmission across electrodes functionalized with diamondoid derivatives.[30] Motivated by this finding, we tackle the following open question: do such diamondoid-DNA nucleotides have unique optical properties as well? To answer this question, we would also need to understand the charge dynamics within such complexes. Investigating these properties will pave the way for a broader range of applications in nanotechnology and biochemistry and also could suggest complementary DNA detection schemes. These schemes can move the applicability of carbon-based nanostructures beyond electronic sensing and may as well enhance their high potential to be used in optoelectronic applications and DNA detectors.

Along these lines, in this work, we use a diamondoid derivative as a probe to detect the DNA nucleotides through optical signals. Also, addressing the charge dynamics will allow for a deeper understanding of the inherent properties of the diamondoid-nucleotide complexes. On the basis of our findings, we will also provide a protocol on assessing numerical quantum mechanical methods in order to predict the charge transfer processes within general nano-bio molecular systems. In order to achieve this, we perform first-principles simulations to study the noncovalent interaction between the nucleotides and the functionalized diamondoid by analyzing the hydrogen-bond strength and the charge transfer processes associated with them.

RESULTS AND DISCUSSION

The main objective of the current study is to use the diamondoid as a probe to optically distinguish the DNA nucleotides. Accordingly, the electronic and optical properties of the functionalized diamondoid interacting with various nucleotides as well as the charge dynamics related to these properties are of interest. The four natural DNA nucleotides (i.e., nucleobases with the sugar phosphate backbone), namely, 2′-deoxyadenosine 5′-monophosphate, 2′-deoxythymidine 5′-monophosphate, 2′-deoxyguanosine 5′-monophosphate, and 2′-deoxycytidine 5′-monophosphate, are considered and are represented here as “A”, “T”, “G”, and “C”, respectively. Our previous studies with diamondoid-functionalized devices have revealed that the high sensitivity of memantine-functionalized electrodes is electronically distinguished among these nucleotides.[29] In view of this, we consider memantine functionalized with a thiol group as a probe for optically interrogating the DNA nucleotide. In general, the thiol group provides the anchor to an electrode material. We will use the notation “memS” for the thiol-functionalized memantine. Memantine is biocompatible and well-known as a drug used in Alzheimer’s disease.[31] The geometries of the isolated molecules, nucleotides and diamondoid, are optimized, and the resulting structures are presented in Figure 1.

Bonding Configurations and Stability of the memS-Nucleotide Complexes. As a first step toward understanding the properties of the memS-nucleotide complexes, we study their structural and binding characteristics. As the nucleobases are aromatic in nature and the memS contains hydrogen-terminated sp^3 carbons along with the NH_2 and SH substitution groups, the interactions are purely noncovalent and are governed by CH$\cdots\pi$, NH$\cdots\pi$, and SH$\cdots\pi$ interactions besides the predominant hydrogen-bonding interactions. The latter interaction is stronger and can potentially be used for

DOI: 10.1021/acsabm.8b00011
ACS Appl. Bio Mater. 2018, 1, 59−69

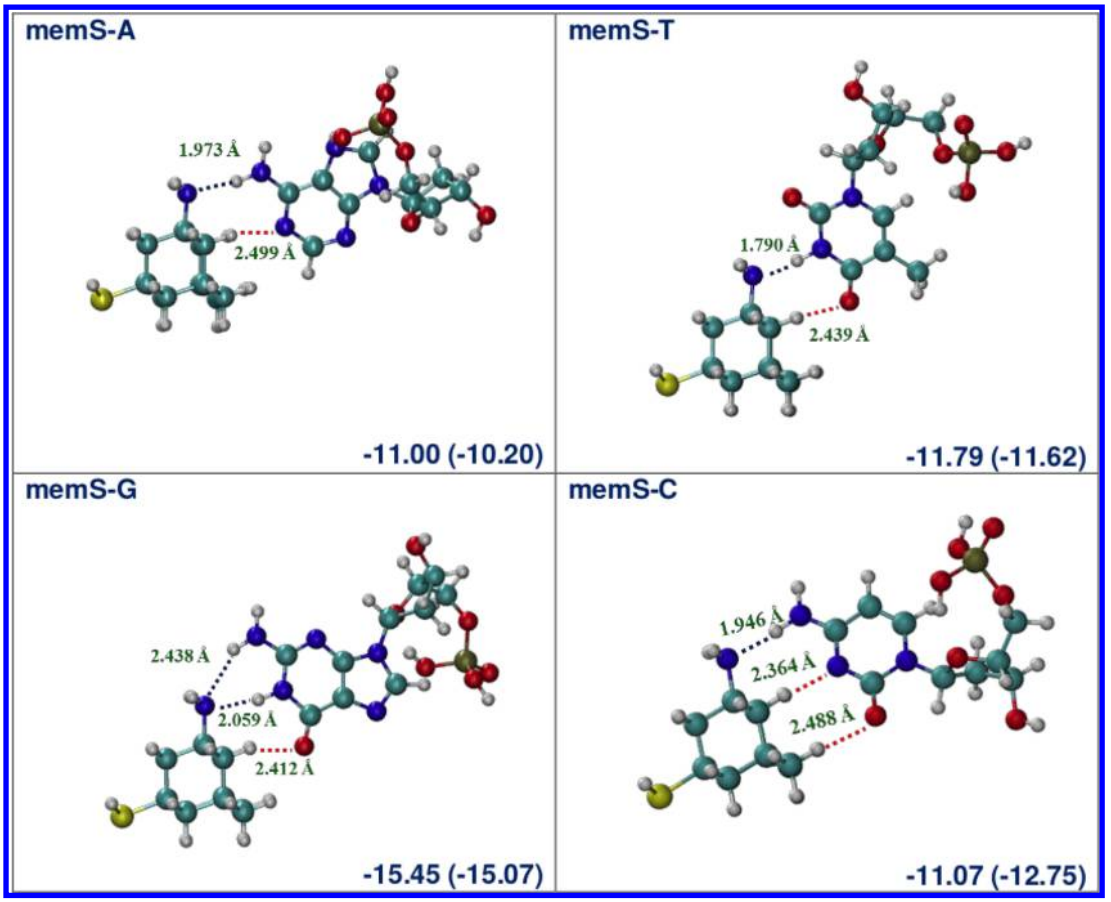

Figure 2. Optimized geometries for the memS-nucleotide complexes and the corresponding interaction energies in kcal/mol, E_{int} (E'_{int}) calculated through eqs 1 and 2). Two distinct type of hydrogen bonds (represented as dotted lines, colored differently) and their lengths are shown. The NH_2 group of the diamondoid is a hydrogen-bond acceptor. The hydrogen bonds involving the NH_2 group are colored blue. The C−H groups act as hydrogen-bond donors and the corresponding hydrogen bonds are colored red.

sensing purposes.[29,32] For sensing, memS will be attached to metallic electrodes through its thiol group, which in turn cannot take part in the binding with a nucleotide. To this aim, here, we only focus on the hydrogen-bonding configurations. Typically, a propeller angle can be defined to study the hydrogen-bond strengths within DNA base pairs and elude the $\pi-\pi$ stacking due to the van der Waals interactions.[33] In the case of the A-T base pair, the propeller angle defined along the C8−C6 axes (see atom labeling in Figure 1) allows the DNA base pair to align in-plane with the most stable geometry and the rotation of the nucleobases along the perpendicular bisector of the C8−C6 axis reduces the hydrogen-bonding interaction. A similar approach is used here by aligning the NH_2 group of memS with respect to the nucleotides.

Figure 2 shows the optimized geometries and the interaction energies for the memS-nucleotide complexes. Figure 2 also shows the hydrogen-bond lengths among the H, N, and O atoms of the memS and the nucleotides. The computed interaction energies reveal that G has the largest interaction with the memS. The interaction energies follow the order: G > C > T > A. In all of these complexes, the amine group of memS acts as a hydrogen-bond acceptor. The memS-G and memS-C complexes are stabilized by three hydrogen bonds, while memS-A and memS-T complexes are stabilized by two hydrogen bonds. In memS-G, a bifurcated hydrogen bond is observed between the nitrogen of memS and the hydrogen atoms of "1N' and '2N" in G (see atom labeling in Figure 1). The binding strengths of memS with nucleotides are in the range of physisorption and chemisorption and can be comparable to the adsorption of nucleobases on graphene.[34] Interestingly, the nucleobases show a higher affinity toward graphene in comparison to the nucleotides affinity to memS. This is essentially due to the strong $\pi-\pi$ interaction between the graphene-nucleobases in contrast to the hydrogen-bonding interaction in memS-nucleotides. Thus, an admissible binding strength of the nucleotides subsequent to adsorption suggests that memS can serve as a promising material for detecting DNA.

In order to confirm that the memS with the NH_2 group as a hydrogen bond (H-bond) acceptor forms the minimum energy configurations with the nucleotides, we also consider memS-nucleotide complexes in which the memS NH_2 group acts as a H-bond donor. The respective optimized geometries and interaction energies are depicted in Figure 3. The interaction energies for the H-bond donor complexes are lower than their respective H-bond acceptor complexes. The difference in energies are in the range 3−7 kcal mol^{-1} except for the memS-T. For these complexes, the NH_2 and C−H groups of memS are aligned perpendicular to the π-cloud of the nucleotides and are predominantly stabilized by a single H-bond and weak dispersion interactions. The difference in relative energies for the two configurations (H-bond donor and H-bond acceptor complexes) is around 3−5 kcal mol^{-1}. In order to estimate the energy required to transit from one

DOI: 10.1021/acsabm.8b00011
ACS Appl. Bio Mater. 2018, 1, 59−69

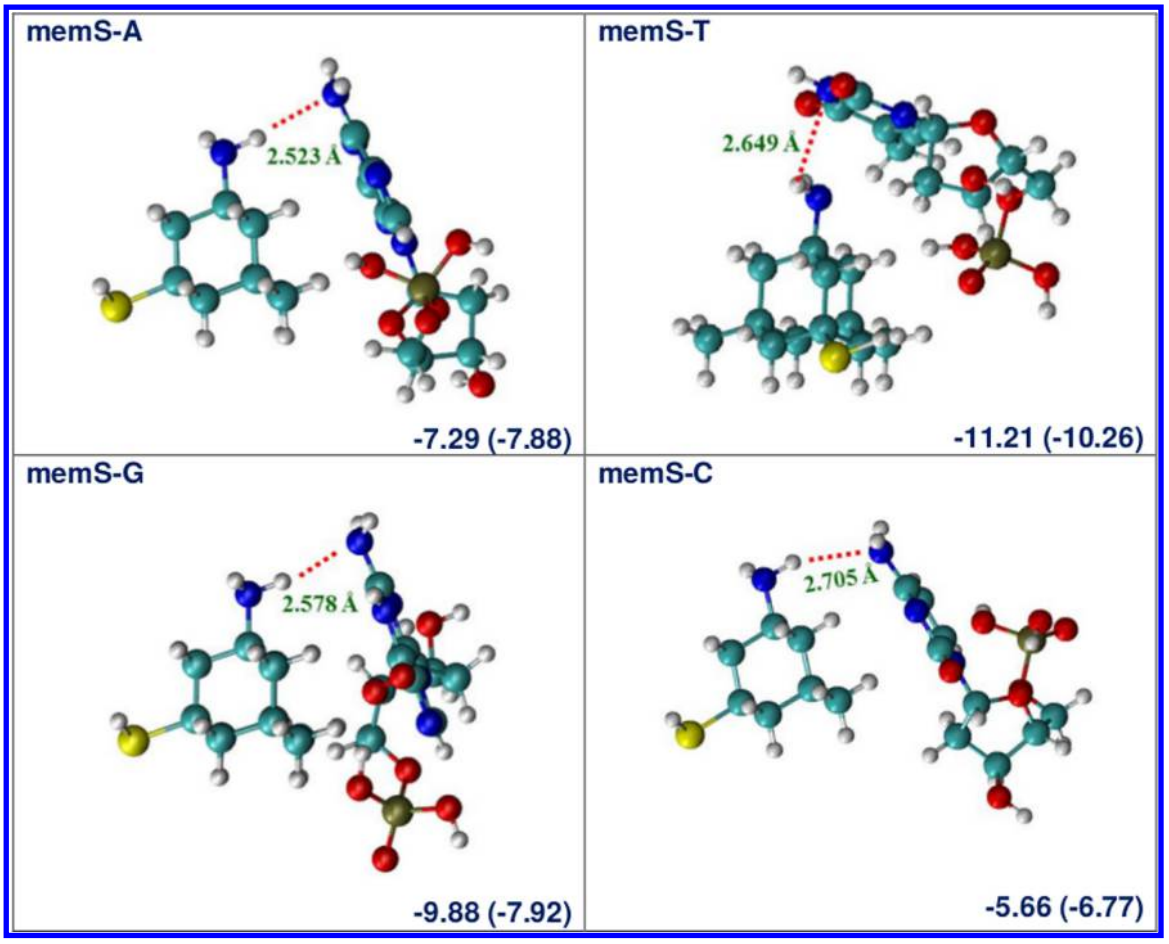

Figure 3. Optimized geometries for the memS-nucleotide complexes and the corresponding interaction energies in kcal/mol, E_{int} (E'_{int}) calculated through eqs 1 and 2. Hydrogen-bond lengths are also shown. The NH_2 group of diamondoid is a hydrogen-bond donor. The corresponding hydrogen bonds are colored red.

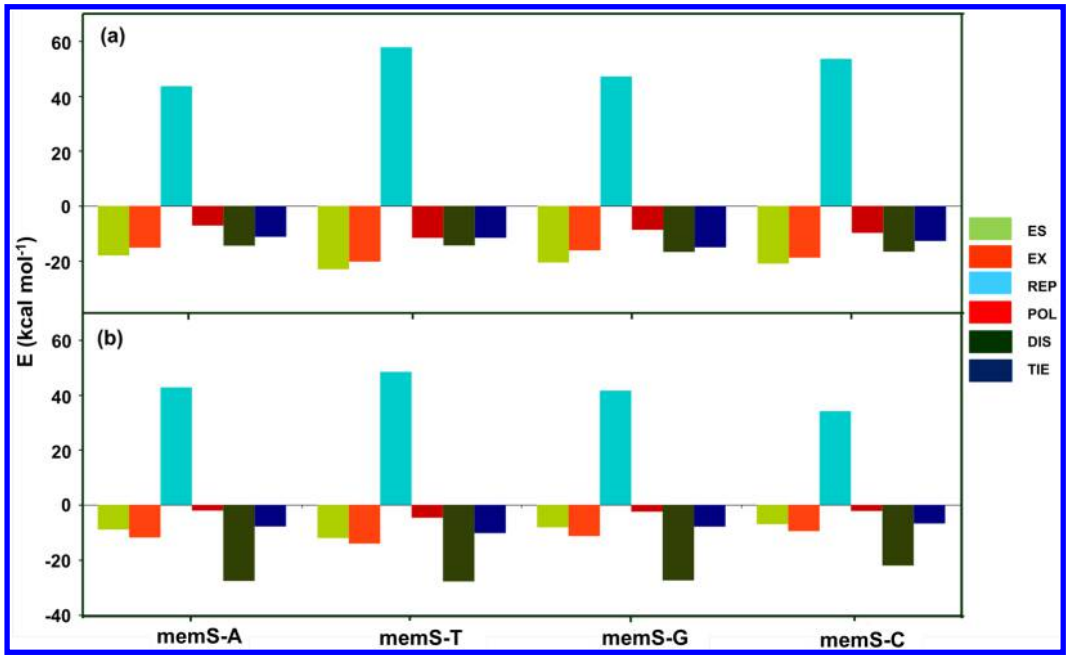

Figure 4. Energy decomposition analysis with the different energy contributions for the memS-nucleotide complexes with memS acting as (a) a hydrogen-bond acceptor and (b) a hydrogen-bond donor. TIE, ES, EX, REP, POL, and DIS denote the total interaction energy, electrostatic, exchange, repulsion, polarization, and dispersion energy, respectively.

DOI: 10.1021/acsabm.8b00011
ACS Appl. Bio Mater. 2018, 1, 59−69

configuration to the other, we have calculated the activation energy for the memS-A complex by employing the Nudge-elastic band (NEB) method as implemented in the NWChem program. Although the relative energies are found to be very low, a high activation barrier of the order of 10^5 kcal mol^{-1} is required for switching from one configuration to another. Hence, the initial geometries play a key role in the stabilization of these nano-bio complexes.

Having analyzed the two possible and stable geometries of the memS-nucleotide complexes, we proceed with the energy decomposition analysis (EDA) of these complexes (see Methodology section). This analysis allows to identify the differences in binding strengths between the two configurations and to study the nature of the interactions. Figure 4 shows the individual energy components for the various memS-nucleotide complexes in both configurations. For the H-bond acceptor complexes, the ES, EX, and DIS components contribute the most to the TIE. In all cases, the contribution from the repulsion term (REP) is relatively high. For the H-bond donor complexes, the ES contributions are decreased by ≈10 kcal mol^{-1}, while DIS contribution is increased by ≈10 kcal mol^{-1} in comparison to the H-bond acceptor complexes. Thus, H-bond donor complexes are stabilized by the dispersion interactions. For the memS-T, although the TIE is similar in both of the configurations, the individual components denote that the H-bond acceptor complex is stabilized by the ES and EX interactions, while the H-bond donor complex is stabilized by the DIS interactions. However, a delicate balance of the large positive values from the REP contribution and the negative values from the other components gives rise to the non-negligible TIE for all these complexes. The H-bond strengths of memS-nucleotides can also be compared with the H-bond of the A-T and G-C base pairs. The H-bond energy of A-T and G-C is 17.0 and 30.0 kcal mol^{-1},[34] respectively, which is higher than the memS-nucleotide complexes. This feature suggests that the memS is an excellent probe for DNA, which will not dissociate or deform the double-strand DNA in contact.

Electronic and Optical Properties. We then perform the molecular orbital analysis for the isolated memS nucleotides and compared the respective features to those of memS-nucleotide complexes. Figure 5 shows the highest occupied molecular orbital (HOMO) and lowest unoccupied molecular orbital (LUMO) for all of these cases. For the isolated memS, the HOMO is delocalized on the amine and thiol groups and across the carbon atoms connecting these groups, while the LUMO is partially localized on the thiol group and the carbon atoms. In the isolated nucleotides, the HOMOs are delocalized around the aromatic rings, while LUMOs show different features for each nucleotide.

In the memS-A and memS-T complexes with memS as a H-bond acceptor, the HOMO and LUMO are localized on the nucleotides, similar to the isolated nucleotides. For the respective memS-G complex, the LUMO is localized on the hydrogen bond between the NH_2 groups of memS and G. For the memS-C, the HOMO is localized on the diamondoid and the LUMO is localized on the nucleotide. Accordingly, the nucleotide type controls the interaction with the memS denoting nucleotide-specific features. The electron density distribution for the H-bond donor complexes is quite uniform: the HOMOs are localized on the diamondoid, and LUMOs are localized on various regions of the nucleotides. The memS-T complex shows an exception with the HOMO being localized on the nucleotide. In order to quantitatively compare all of the

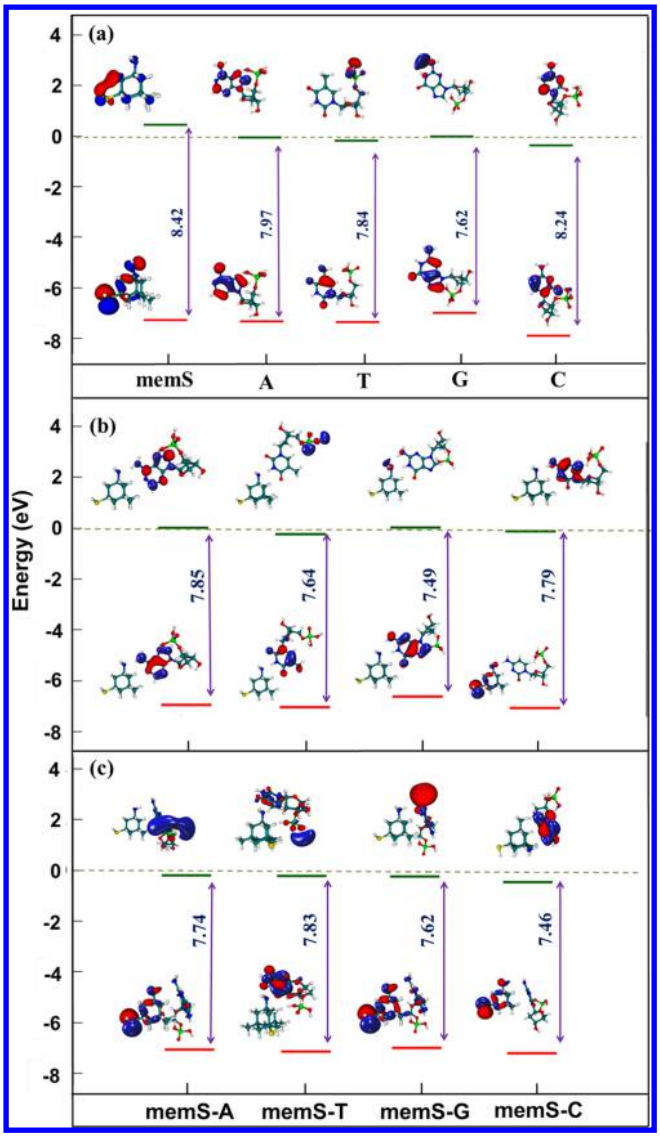

Figure 5. Frontier molecular orbitals. HOMO and LUMO are denoted by the red and green horizontal lines, respectively. The blue numbers in the graphs are the H-L gaps in eV. Panel a includes the features for all isolated molecules (memS, A, T, G, C). Panels b and c include the feature for the memS-nt complexes, in which memS acts as a H-bond acceptor and H-bond donor, respectively.

complexes, we have calculated the HOMO−LUMO (H-L) gaps for the isolated and the memS-nucleotide complexes. For the isolated molecules, the memS shows the higher H-L gap than the nucleotides. In the complexes, the H-L gaps are lower than their respective isolated nucleotides and differ with respect to the nucleotide type. The difference in the H-L gaps for the different configurations is between 0.1 and 0.3 eV, which is indeed due to the relative arrangements and the bonding characteristics of the memS interaction with the nucleotides. The differences in the H-L gaps of the complexes for different nucleotides demonstrate preserved intrinsic properties of the nucleotides on interaction with memS. This finding indicates nucleotide-specific features and can be expected to be observed in other properties, like the optical ones. Thus, memS could be used to tune and enhance the differences among the nucleotides in view of sensing.

DOI: 10.1021/acsabm.8b00011
ACS Appl. Bio Mater. 2018, 1, 59−69

Along the lines above, we continue with the optical properties of the memS-nucleotide complexes and calculate the respective absorption spectra. The results from the LR-TDDFT calculations are presented in Figure 6 for the isolated

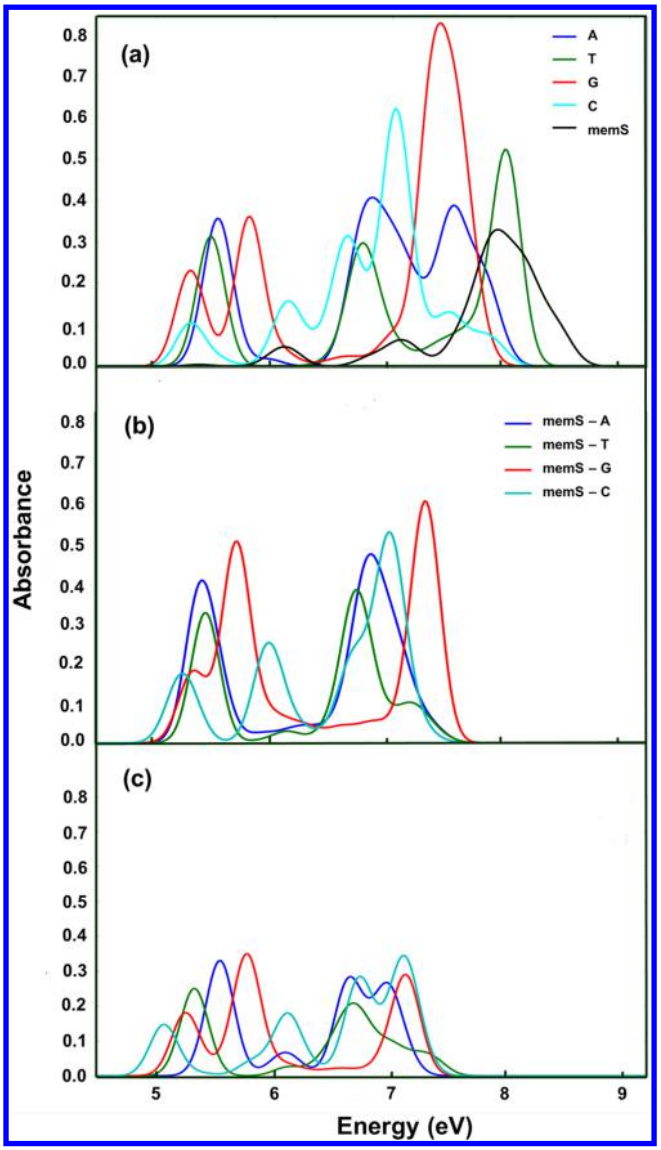

Figure 6. Absorption spectra of (a) the isolated nucleotides and diamondoid, (b) the diamondoid-nucleotide complexes with memS as a H-bond acceptor, and (c) the complexes with memS as a H-bond donor.

molecules and the complexes in both configurations. The computed absorption spectra for the nucleotides are in the range between 5 and 8 eV, which agree well with the experiments, taking into account a shift of about 1 eV.[35,36] From Figure 1, we observe that the spectral range for the isolated memS and the nucleotides is similar. Interestingly, no significant shift in the absorption spectra is observed for the memS-nucleotide complexes except a decrease in the oscillator strengths at higher energy. This decrease is related to the pronounced peak of the isolated memS at higher energies, at which it is significantly interacting with the nucleotides. The excitation energy differences between the isolated nucleotides and the memS-nucleotide complexes are very small due to the weak interactions between the memS and the nucleotides. Additionally, the features in the absorption spectra of the memS-nucleotide complexes are dominated by the nucleotides. This is essentially due to the presence of electron-rich parts in the nucleotides (in comparison to memS), which participate in the electronic excitation. Note that in the neutral complexes no charge transfer between the memS and the nucleotides is observed. The excitation energy difference can be controlled by tuning the specific interactions of the probe molecule with the nucleotides. This could be done, for example, through a broader search for a probe molecule. The exploration of overlapped bands in the absorption spectra provides invaluable information about the structure of the molecule and its environment.[35,37] In contrast to the isolated nucleotides, the complexes where memS is a hydrogen-bond acceptor show a pronounced band overlap. No such band overlap is observed for the complexes in which memS is the hydrogen-bond donor. Accordingly, qualitative differences between the isolated nucleotides and various bonding configurations of the memS-nucleotide complexes can be identified from the absorption spectra.

In order to further quantify the spectral features, the lowest vertical excitation energy and the corresponding oscillator strength for the isolated memS and nucleotides, as well as the memS-nucleotides complexes, are summarized in Table 1. The

Table 1. Calculated Lowest Vertical Excitation Energies (ΔE_{abs}, As Defined Previously[38]) with the Oscillator Strength (f, in Arbitrary Units) of the Major Contribution to the Allowed Transitions for the Ideal memS, Nucleotides, and All Complexes from Figures 1 and 2[a]

	ΔE_{abs} (eV)	oscillator strength (f)	major contributions	exp[36]
memS	5.361	0.004	H→L	
A	5.431	0.015	H→L+1	4.59
T	5.459	0.313	H→L+1	4.5−4.7
G	5.272	0.192	H→L, H→L+2	4.4−4.5
C	5.286	0.103	H→L	4.6
		H-bond acceptor		
memS-A	5.361	0.345	H→L	
memS-T	5.416	0.323	H→L+1	
memS-G	5.306	0.171	H→L+5	
memS-C	5.185	0.116	H-1→L	
		H-bond donor		
memS-A	5.511	0.142	H-1→L+1	
memS-T	5.313	0.245	H→L+1	
memS-G	5.236	0.178	H-1→L+2	
memS-C	5.050	0.146	H-2→L	

[a]Experimental vertical excitation energies (exp) for the ideal nucleobases are also provided for comparison.[36]

allowed transitions for the excitation states, i.e., the highly contributing molecular orbitals, are also given. "H→L" denotes a transition from the HOMO to the LUMO level. The lowest vertical excitation energy for the isolated nucleotides is in agreement with the experiments, with a shift of about 1 eV.[35,36] The shift in the computed values in comparison to the measured values is due to the choice of the functional as well as the finiteness of the basis set. In order to understand these differences, we should have in mind that in our calculations the nucleotides are considered in vacuo, while in the experiments the optical transitions vary significantly depending on the surrounding environment of the molecules. (Please see ref 35

DOI: 10.1021/acsabm.8b00011
ACS Appl. Bio Mater. 2018, 1, 59−69

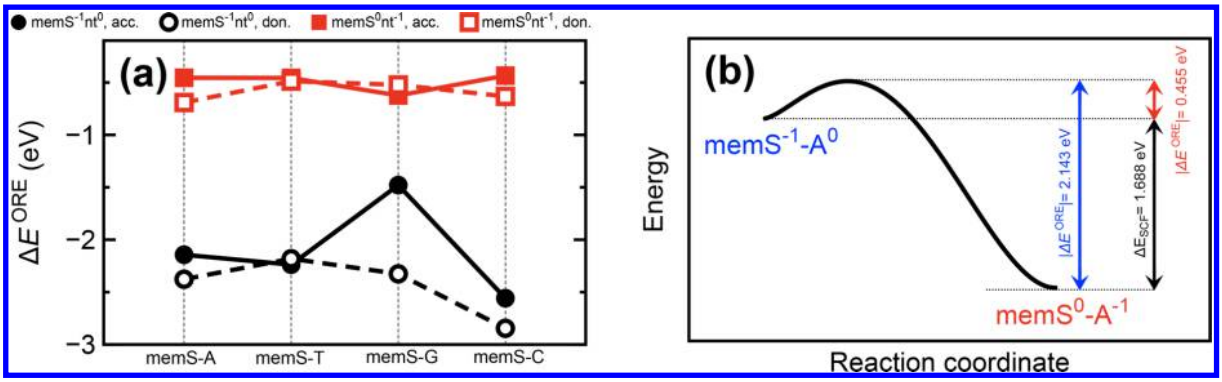

Figure 7. (a) Orbital relaxation energies for the complexes studied here as denoted along the *x*-axis. The solid (open) symbols correspond to the complexes in which memS acts as a H-bond acceptor, "acc" (H-bond donor, "don"). The circles (squares) denote the memS^{-1}nt^0 (memS^{0}nt^{-1}) initial charge configuration. (b) Total energy difference after the orbital relaxation, ΔE_{SCF}, as well as the absolute values of the orbital relaxation energies, $|\Delta E^{ORE}|$, for the memS^{-1}-A^0 (blue) and the memS^0-A^{-1} (red) charge configurations for the diamondoid in the H-bond acceptor conformation.

and the references therein.) For all of the complexes, we notice that the lower excitation energy corresponds to the $\pi \rightarrow \pi^*$ transition within the nucleotides. The $\sigma \rightarrow \pi^*$ transitions from the diamondoid to a nucleotide are observed at higher energy levels. The lowest vertical excitation energies of the complexes lie in the same range as of the isolated molecules and small nucleotide specificity is evident from the differences in ΔE_{abs}. These differences are probably below the resolution limit in the experiments, but show an enhanced potential as discussed for the absorption spectra. This enhancement can be achieved through an optimal choice of the probe molecule interacting with the nucleotides.

Charge Transfer Dynamics. Having assessed the absorption properties of the diamondoid-nucleotide complexes, we move to the study of charge transfer processes within these complexes using the RT-TDDFT method. Understanding the mechanism of such processes is essential in electronic applications. In the charge transfer simulations, both H-bond configurations are studied and the calculations are performed on neutral structures. First, the orbital relaxation energies for the memS^{-1}nt^0 and memS^{0}nt^{-1} electronic charge configurations are calculated. For convenience, we denote the different nucleotides A, T, G, and C as "nt" and the superscripts show the extra local charges. All orbital relaxation energies are summarized in Figure 7a. The orbital relaxation energies are more substantial in the case of the reduced diamondoid, namely, memS^{-1}nt^0. As seen in Figure 7b for the case of the memS-A complex, the absolute values of the orbital relaxation energies corresponding to the charge configuration memS^{0}nt^{-1}, can be viewed as a measure for the charge transfer barrier from the memS^{-1} to nt^0. As such, the smaller absolute values in Figure 7a, that is the red data points, show the possibility of a charge transfer from memS^{-1} to nt^0. Similarly, the black points, with higher absolute values, correspond to the charge transfer from the nt^{-1} to the memS^0 and indicate lower possibilities for the charge transfer processes in the reverse direction. However, there is an exception, namely, the memS^{-1}-G^0 system. The orbital relaxation energy corresponding to this charge configuration has a lower absolute value, which demonstrates the possibility of a charge transfer process from G^{-1} to memS^0. As such, the orbital relaxation energies can provide an estimation on the direction of charge transfer processes.

In order to visualize the charge dynamics within the diamondoid-nucleotides, in Figure 8, we first present the

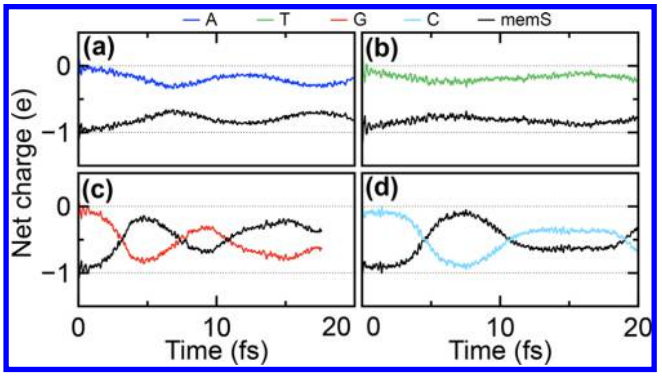

Figure 8. Charge oscillations within the diamondoid-nucleotide complexes with the memS as a H-bond acceptor and initial charge configurations of (a) memS^{-1}A^0, (b) memS^{-1}T^0, (c) memS^{-1}G^0, and (d) memS^{-1}C^0.

results for the H-bond acceptor complexes. As evident from the figure, charge transfer only occurs in the case of the G and C nucleotides. The charge oscillations occur on ∼5 and ∼8 fs time scales for memS-G and memS-C, respectively. Similarly, the charge dynamics for the H-bond donor complexes are shown in Figure 9. The charge transfer is observed between the diamondoid and A, C, and G. However, the charge transfer processes in these complexes do not show Rabi oscillations. The one-way electron transfer occurs in less than 1 fs from the

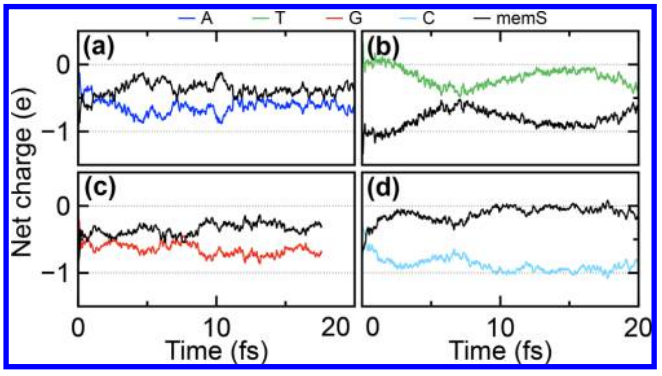

Figure 9. Charge transfer dynamics within the diamondoid-nucleotide complexes with the memS as a H-bond donor and initial charge states of (a) memS^{-1}A^0, (b) memS^{-1}T^0, (c) memS^{-1}G^0, and (d) memS^{-1}C^0.

DOI: 10.1021/acsabm.8b00011
ACS Appl. Bio Mater. 2018, 1, 59−69

diamondoid to the nucleotides. In the case of memS-C, the additional electron is almost completely transferred to C. However, in the memS-A and memS-G complexes, the additional charge is almost equally shared between the molecules. The initially imposed charge configurations, $memS^{-1}nt^{0}$, result in a two-level electronic state, which can be considered as a superposition of the HOMO and the LUMO orbitals of each complex. Accordingly, in every case where the HOMO and LUMO orbitals of the neutral complex are localized on different molecules, a charge transfer can be observed. As shown in Figure 5b and 5c, this is the case for memS-G and memS-C in the H-bond acceptor configurations, and memS-A, memS-G, and memS-C in the H-bond donor configurations.

As shown above, the orbital relaxation energies in Figure 7 indicate that the electron transfer is more likely to occur from the diamondoid to the nucleotides. The same analysis also signals the possibility of electron transfer from the nucleotide to the diamondoid in the memS-G complex. In order to test our observations, we explicitly inspected the possibility of the electron transfer from the nucleotide to the diamondoid in two cases: the memS-G and the memS-C complexes in both H-bond acceptor and H-bond donor configurations. For this, $memS^{0}nt^{-1}$ are the initial charge configurations. The results presented in Figure 10 lead to no charge transfer for the memS-C complex irrespective of its structural configurations. On the other hand, a charge oscillation in the H-bond acceptor configuration of the memS-G complex is observed again with a time scale comparable to that in Figure 8c. However, as predicted in the orbital relaxation energy analysis (Figure 7), no charge transfer from the nucleotides to the diamondoid is observed in the H-bond donor configuration of the memS-G complex.

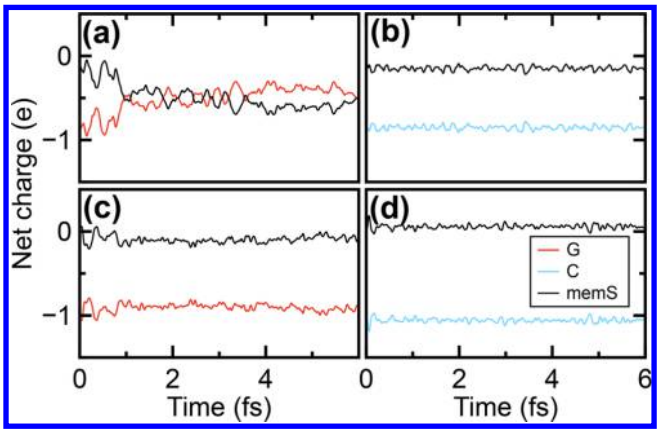

Figure 10. Charge transfer dynamics within the diamondoid-nucleotide complexes in $memS^{0}nt^{-1}$ starting charge configuration. Panels a and c show the charge dynamics for the memS-G, and panels b and d present that for the memS-C complex. Panels a and b correspond to the complexes with the diamondoid in the H-bond acceptor conformation, while panels c and d correspond to the diamondoid being the H-bond donor.

In order to have a better understanding of the charge transfer mechanism, we also performed charge transfer simulations on a simple adenine-thymine base pair. The charge transfer simulation in this base pair with a $adenine^{-1}thymine^{0}$ initial charge configuration results in an oscillatory behavior depicted in Figure 11. (Note that herein we considered the adenine and thymine nucleobases without sugar phosphate groups as

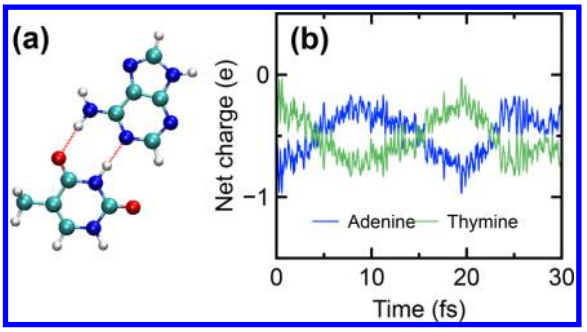

Figure 11. (a) Optimized neutral configuration of the adenine-thymine base pair. The hydrogen bonds are shown in dashed red lines. (b) Charge oscillations between adenine and thymine. The initial charge configuration was $adenine^{-1}thymine^{0}$.

considered in the rest of this study.) The initial charge configuration was chosen based on the orbital relaxation energies, namely, −1.25 eV for the $adenine^{-1}thymine^{0}$ and −0.5 eV for the $adenine^{0}thymine^{-1}$ configurations. In the adenine-thymine base pair, each molecule interacts with the other through two different hydrogen bonds. In this way, each molecule is donating one proton and simultaneously accepting another proton from the H-bond. This denotes a mechanism in which the electronic flow first occurs from adenine to thymine through the NH···O bond followed by a back flow from thymine to adenine via NH···N. Extrapolating this evidence to the diamondoid-nucleotide complexes indicates that the oscillatory charge dynamics in the H-bond acceptor complexes must be due to the existence of both types of H-bonds, while, in the H-bond donor complexes due to a single hydrogen bond, we only observe a one-way electron transfer. One should also note that the charge transfer processes in both H-bond donor and H-bond acceptor complexes occur rather fast. This indicates that the effect of nuclear motion on the observed charge transfer mechanism is minimal.

CONCLUSIONS

The nano-bio complexes studied here can be viewed as essential building blocks in nanomaterials and applications, which involve probing biomolecules with nanostructures. Along these lines, we have carried out quantum mechanical investigations on diamondoid/nucleotide complexes in order to unravel their fundamental properties and relevance to biosensing. With the current study, we provide additional insight on the optical properties of the complexes as an additional protocol for sensing the nucleotide identity. We have considered two configurations of the complexes, which give rise to different binding strengths. For most of the cases, the role the diamondoids as the hydrogen-bond acceptor leads to more stable complexes.

A frontier orbital analysis revealed that the HOMO−LUMO gap of the diamondoid-nucleotides complexes are slightly different from that of the isolated nucleotides. This clearly manifests the nucleotide-specific electronic features of the complexes. Their optical properties show a small shift in the absorption peaks relative to the isolated nucleotides. Depending on the binding arrangement of the complexes, a decrease in the intensity of the absorption peaks at a higher energy is observed. This indicates that there is still room to enhance the nucleotide specificity with other probe molecules for optically detecting DNA. The charge dynamics in the complexes can be observed in the femtosecond scale and depend on the relative

DOI: 10.1021/acsabm.8b00011
ACS Appl. Bio Mater. 2018, 1, 59−69

arrangement of the molecules and the nucleotide identity. The oscillatory or one-way charge transfer behavior between the diamondoid and the nucleotides was found to correlate to the nature of the hydrogen bonding in the complex. Accordingly, our results clearly demonstrate the importance of the conformational details on the charge dynamics in hybrid nano-bio systems.

In the end, we should note that additional factors, such as a solvent, electric field, and finite temperature, influence the diamondoid/nucleotide properties. The interplay of these factors and their effect on the reported results should be further evaluated. Nevertheless, the novelty of this work is related to (a) the choice of the nano-bio system, namely, diamondoid-nucleotide complexes, and (b) the suggestion of an approach to understand (and possibly predict) the charge transfer dynamics of such systems avoiding expensive calculations. This can be proven to be very efficient in numerical investigations of molecular systems and can provide invaluable input to experiments for the realization of novel biosensing applications and biomaterials.

METHODOLOGY

All of the quantum mechanical calculations are carried out based on density functional theory (DFT).[39,40] The geometry optimizations for the various complexes are performed using the dispersion-including DFT with a Pople basis set of polarized triple-ζ basis functions. The ground-state electronic properties are carried out using the M06-2X functional.[41] This functional provides a good description of the long-range dispersive forces and has earlier been used to model the interactions of nucleobases with graphene and CNTs.[42,43] The results obtained using this functional are found to be in agreement with the experiments. The initial geometry optimizations of the structures are performed using the 6-31G(d,p) basis set, followed by single-point energy calculations at the 6-311+G(d,p) level with the same functional (M06-2X/6-311+G(d,p)//M06-2X/6-31G(d,p)). The vibrational frequency analysis is carried out to ensure that the obtained geometries represent the minimum-energy configuration on the potential energy surface. All of the ground state geometry optimizations are performed using the code Gamess-US.[44,45]

As a measure of the binding strengths between the diamondoid and the nucleotide, the interaction energy is computed using two methods. In method I, the interaction energies are calculated as

$$E_{\mathrm{int}} = E_{\mathrm{complex}} - E_{\mathrm{diamondoid}} - E_{\mathrm{nucleotides}} \quad (1)$$

where E_{complex}, $E_{\mathrm{diamondoid}}$, and $E_{\mathrm{nucleotides}}$ are the energies of the optimized geometries of the diamondoid-nucleotide complexes, isolated diamondoid, and isolated nucleotides, respectively. In method II, the interaction energies are computed as

$$E'_{\mathrm{int}} = E_{\mathrm{complex}} - E'_{\mathrm{memS}} - E'_{\mathrm{nucleotides}} \quad (2)$$

where E'_{memS} and $E'_{\mathrm{nucleotides}}$ are the single-point energies of the isolated diamondoid and the isolated nucleotides in the corresponding complexes, respectively. The E'_{int} are corrected for the basis set superposition error using the counterpoise method.[46]

The functionalized diamondoid and the nucleotides interact with each other through noncovalent interactions, which involve electrostatics, hydrogen bonding (H-bond), and dispersion interactions. These interactions can be further probed by performing energy-decomposition analysis (EDA).[47] EDA is an effective tool that decomposes the total interaction energy (TIE) into its components such as electrostatics (ES), exchange (EX), repulsion (REP), polarization (POL), and dispersion (DIS). The EDA is performed using the localized molecular orbital EDA (LMOEDA) as implemented in GAMESS-US at the M06-2X/6-311+G(d,p)//M06-2X/6-31G(d,p) level of theory. The total interaction energy (ΔE_{TIE}) is written as a sum of electrostatic (ΔE_{ES}), exchange (ΔE_{EX}), repulsion (ΔE_{REP}), polarization (ΔE_{POL}), and dispersion (ΔE_{DIS}) components and is given by

$$\Delta E_{\mathrm{TIE}} = \Delta E_{\mathrm{ES}} + \Delta E_{\mathrm{EX}} + \Delta E_{\mathrm{REP}} + \Delta E_{\mathrm{POL}} + \Delta E_{\mathrm{DIS}} \quad (3)$$

For the optical properties of the diamondoid-nucleotides complexes, the linear response time-dependent DFT (LR-TDDFT)[48] is employed using the CAM-B3LYP functional[49] with 6-31+G(d) basis set to calculate the electronic excitations as well as their associated states (CAM-B3LYP/6-31+G(d)//M06-2X/6-31G(d,p)). TDDFT has been demonstrated to be a powerful and efficient tool for evaluating the low-lying excited-state spectra of small organic molecules. It has the ability to predict accurate absorption spectra in line with the experiments at a relatively low computation cost.

The CAM-B3LYP range-separated functional[49] was earlier used to ensure the correct asymptotic behavior of the exchange energy,[49−54] which is crucial for an accurate estimation of long-range charge transfer energies between interacting molecules. Herein, we study the electron transfer processes between the diamondoid and the nucleotides using a real-time approach to the TDDFT (RT-TDDFT)[53] as implemented in NWChem.[55] The RT-TDDFT method has been successfully employed to investigate the charge transfer between organic and inorganic molecules.[56,57] The Ahlrichs Coulomb fitting basis set is used in the RT-TDDFT simulations to compute the Coulomb part of the Fock matrix.[58] The initial charge configurations of the complexes are constructed by combining the ground-state molecular orbitals of separate individual molecules, where one of the molecules has a −1.0 charge, while the other is neutral. For each complex, the orbital relaxation energies corresponding to the imposed charge configuration are calculated as well. The orbital relaxation energies can be viewed as a measure for the stability of the final charge configuration during a charge transfer process. The orbital relaxation energies are defined as

$$\Delta E^{\mathrm{ORE}} = E_0 - E_{\mathrm{SCF}} \quad (4)$$

where E_{SCF} is the total energy of the charged system after orbital relaxation, while the total energy of the charged system in zeroth approximation, E_0, is written as

$$E_0 = E_{\mathrm{SCF}}^{\mathrm{neutral}} + \epsilon_i \quad (5)$$

$E_{\mathrm{SCF}}^{\mathrm{neutral}}$ is the total energy of the neutral complex, and ϵ_i is the energy of i^{th} molecular orbital to be filled with one extra electron. For orbital relaxation energy calculations, the initial charge configurations are imposed using constrained DFT[59] along with the 6-31G* basis set.

AUTHOR INFORMATION

Corresponding Author

*E-mail: pouya.partovi-azar@chemie.uni-halle.de.

ORCID

Chandra Shekar Sarap: 0000-0002-8621-6800

DOI: 10.1021/acsabm.8b00011
ACS Appl. Bio Mater. 2018, 1, 59−69

Pouya Partovi-Azar: 0000-0001-5568-1315

Notes

The authors declare no competing financial interest.

■ ACKNOWLEDGMENTS

C.S.S. and M.F. acknowledge financial support from the Junior Professoren Programm funded by the Ministry of Science, Research and the Arts Baden-Württemberg (MWK). Funding from the SFB716 collaborative network "Dynamic simulation of systems with large particle numbers" of the Deutsche Forschungsgemeinschaft (DFG) and the CRC SimTech Cluster at the University of Stuttgart is also greatly acknowledged. This research was supported in part by the bwHPC initiative and the bwHPC-C5 project provided through associated compute services of the JUSTUS HPC facility at the University of Ulm. The bwHPC and bwHPC-C5 (http://www.bwhpc-c5.de) are funded by the Ministry of Science, Research and the Arts Baden-Württemberg (MWK) and the German Research Foundation (DFG). Part of this work was also performed on the computational resource ForHLR Phase II funded by the Ministry of Science, Research and the Arts Baden-Württemberg and DFG. P.P.-A. gratefully acknowledges Prof. D. Sebastianii for fruitful discussions.

■ REFERENCES

(1) Willner, I.; Willner, B. Biomolecule-based Nanomaterials and Nanostructures. *Nano Lett.* **2010**, *10*, 3805−3815.
(2) *Nanostructures for Novel Therapy*; Ficai, D., Grumezescu, A. M., Eds.; Elsevier: 2017.
(3) Zhu, Y.; Murali, S.; Cai, W.; Li, X.; Suk, J. W.; Potts, J. R.; Ruoff, R. S. Graphene and Graphene Oxide: Synthesis, Properties, and Applications. *Adv. Mater.* **2010**, *22*, 3906−3924.
(4) Inagaki, M.; Kang, F. Graphene Derivatives: Graphane, Fluorographene, Graphene Oxide, Graphyne and Graphdiyne. *J. Mater. Chem. A* **2014**, *2*, 13193−13206.
(5) Partovi-Azar, P.; Namiranian, A. Stone−Wales Defects can Cause a Metal−semiconductor Transition in Carbon Nanotubes Depending on their Orientation. *J. Phys.: Condens. Matter* **2012**, *24*, 035301.
(6) Partovi-Azar, P.; Jand, S. P.; Namiranian, A.; Rafii-Tabar, H. Electronic Features Induced by Stone−Wales Defects in Zigzag and Chiral Carbon Nanotubes. *Comput. Mater. Sci.* **2013**, *79*, 82−86.
(7) Partovi-Azar, P.; Jand, S. P.; Kaghazchi, P. Electronic, Magnetic, and Transport Properties of Polyacrylonitrile-based Carbon Nanofibers of Various Widths: Density-Functional Theory Calculations. *Phys. Rev. Appl.* **2018**, *9*, 014012.
(8) Lu, Y.; Lerner, M. B.; Qi, Z. J.; Mitala, J. J., Jr.; Lim, J. H.; Discher, B. M.; Johnson, A. T. C. Graphene-Protein Bioelectronic Devices with Wavelength-Dependent Photoresponse. *Appl. Phys. Lett.* **2012**, *100*, 033110.
(9) Luan, B.; Zhou, R. Nanopore-Based Sensors for Detecting Toxicity of a Carbon Nanotube to Proteins. *J. Phys. Chem. Lett.* **2012**, *3*, 2337−2341.
(10) Liu, Y.; Dong, X.; Chen, P. Biological and Chemical Sensors Based on Graphene Materials. *Chem. Soc. Rev.* **2012**, *41*, 2283−2307.
(11) Lu, Y.; Goldsmith, B. R.; Kybert, N. J.; Johnson, A. T. C. DNA-decorated Graphene Chemical Sensors. *Appl. Phys. Lett.* **2010**, *97*, 083107.
(12) Weizmann, Y.; Chenoweth, D. M.; Swager, T. M. DNA-CNT Nanowire Networks for DNA Detection. *J. Am. Chem. Soc.* **2011**, *133*, 3238−3241.
(13) Jin, Z.; Sun, W.; Ke, Y.; Shih, C.-J.; Paulus, G. L. C.; Hua Wang, Q.; Mu, B.; Yin, P.; Strano, M. S. Metallized DNA Nanolithography for Encoding and Transferring Spatial Information for Graphene Patterning. *Nat. Commun.* **2013**, *4*, 1−9.
(14) Chandra Shekar, S.; Swathi, R. S. Stability of Nucleobases and Base Pairs Adsorbed on Graphyne and Graphdiyne. *J. Phys. Chem. C* **2014**, *118*, 4516−4528.
(15) Balaban, A. T.; Schleyer, P. V. R. Systematic Classification and Nomenclature of Diamond Hydrocarbons-I. *Tetrahedron* **1978**, *34*, 3599−3609.
(16) Dahl, J. E.; Liu, S. G.; Carlson, R. M. K. Isolation and Structure of Higher Diamondoids, Nanometer-Sized Diamond Molecules. *Science* **2003**, *299*, 96−99.
(17) Schwertfeger, H.; Fokin, A.; Schreiner, P. Diamonds are a Chemist's Best Friend: Diamondoid Chemistry Beyond Adamantane. *Angew. Chem., Int. Ed.* **2008**, *47*, 1022−1036.
(18) Zhou, Y.; Brittain, A. D.; Kong, D.; Xiao, M.; Meng, Y.; Sun, L. Derivatization of Diamondoids for Functional Applications. *J. Mater. Chem. C* **2015**, *3*, 6947−6961.
(19) Demján, T.; Vörös, M.; Palummo, M.; Gali, A. Electronic and Optical Properties of Pure and Modified Diamondoids Studied by Many-body Perturbation Theory and Time-dependent Density Functional Theory. *J. Chem. Phys.* **2014**, *141*, 064308.
(20) Rander, T.; Staiger, M.; Richter, R.; Zimmermann, T.; Landt, L.; Wolter, D.; Dahl, J. E.; Carlson, R. M. K.; Tkachenko, B. A.; Fokina, N. A.; Schreiner, P. R.; Möller, T.; Bostedt, C. Electronic Structure Tuning of Diamondoids through Functionalization. *J. Chem. Phys.* **2013**, *138*, 024310.
(21) Fokin, A. A.; Schreiner, P. R. Band Gap Tuning in Nanodiamonds: First Principle Computational Studies. *Mol. Phys.* **2009**, *107*, 823−830.
(22) Adhikari, B.; Fyta, M. Towards Double-functionalized Small Diamondoids: Selective Electronic Band-gap Tuning. *Nanotechnology* **2015**, *26*, 035701.
(23) Yang, W. L.; Fabbri, J. D.; Willey, T. M.; Lee, J. R. I.; Dahl, J. E.; Carlson, R. M. K.; Schreiner, P. R.; Fokin, A. A.; Tkachenko, B. A.; Fokina, N. A.; Meevasana, W.; Mannella, N.; Tanaka, K.; Zhou, X. J.; van Buuren, T.; Kelly, M. A.; Hussain, Z.; Melosh, N. A.; Shen, Z.-X. Monochromatic Electron Photoemission from Diamondoid Monolayers. *Science* **2007**, *316*, 1460−1462.
(24) Wang, Y.; Kioupakis, E.; Lu, X.; Wegner, D.; Yamachika, R.; Dahl, J. E.; Carlson, R. M. K.; Louie, S. G.; Crommie, M. F. Spatially Resolved Electronic and Vibronic Properties of Single Diamondoid Molecules. *Nat. Mater.* **2008**, *7*, 38−42.
(25) Zhang, G. Diamondoid Molecules: With Applications in Biomedicine, Materials Science, Nanotechnology and Petroleum Science. *Phys. Today* **2013**, *66*, 59−60.
(26) Clay, W. A.; Dahl, J. E. P.; Carlson, R. M. K.; Melosh, N. A.; Shen, Z.-X. Physical Properties of Materials Derived from Diamondoid Molecules. *Rep. Prog. Phys.* **2015**, *78*, 016501.
(27) Lamoureux, G.; Artavia, G. Use of the Adamantane Structure in Medicinal Chemistry. *Curr. Med. Chem.* **2010**, *17*, 2967−2978.
(28) Geldenhuys, W. J.; Malan, S. F.; Bloomquist, J. R.; Marchand, A. P.; Van der Schyf, C. J. Pharmacology and Structure-activity Relationships of Bioactive Polycyclic Cage Compounds: A Focus on Pentacycloundecane Derivatives. *Med. Res. Rev.* **2005**, *25*, 21−48.
(29) Sivaraman, G.; Amorim, R. G.; Scheicher, R. H.; Fyta, M. Benchmark Investigation of Diamondoid-functionalized Electrodes for Nanopore DNA Sequencing. *Nanotechnology* **2016**, *27*, 414002−7.
(30) Sivaraman, G.; Amorim, R. G.; Scheicher, R. H.; Fyta, M. Diamondoid-functionalized Gold Nanogaps as Sensors for Natural, Mutated, and Epigenetically Modified DNA Nucleotides. *Nanoscale* **2016**, *8*, 10105−10112.
(31) Robinson, D. M.; Keating, G. M. Memantine: A Review of Its Use in Alzheimer's Disease. *Drugs* **2006**, *66*, 1515−1534.
(32) Branton, D.; Deamer, D. W.; Marziali, A.; Bayley, H.; Benner, S. A.; Butler, T.; Di Ventra, M.; Garaj, S.; Hibbs, A.; Huang, X.; Jovanovich, S. B.; Krstic, P. S.; Lindsay, S.; Ling, X. S.; Mastrangelo, C. H.; Meller, A.; Oliver, J. S.; Pershin, Y. V.; Ramsey, J. M.; Riehn, R.; Soni, G. V.; Tabard-Cossa, V.; Wiggin, M.; Schloss, J. A.; Wanunu, M. The Potential and Challenges of Nanopore Sequencing. *Nat. Biotechnol.* **2008**, *26*, 1146−1153.

DOI: 10.1021/acsabm.8b00011
ACS Appl. Bio Mater. 2018, 1, 59−69

(33) Cooper, V. R.; Thonhauser, T.; Langreth, D. C. An Application of the van der Waals Density Functional: Hydrogen Bonding and Stacking Interactions between Nucleobases. *J. Chem. Phys.* **2008**, *128*, 204102.
(34) Antony, J.; Grimme, S. Structures and Interaction Energies of Stacked Graphene-Nucleobase Complexes. *Phys. Chem. Chem. Phys.* **2008**, *10*, 2722−2729.
(35) Barbatti, M.; Aquino, A. J. A.; Lischka, H. The UV Absorption of Nucleobases: Semi-classical Ab Initio Spectra Simulations. *Phys. Chem. Chem. Phys.* **2010**, *12*, 4959−4967.
(36) Varsano, D.; Di Felice, R.; Marques, M. A. L.; Rubio, A. A TDDFT Study of the Excited States of DNA Bases and Their Assemblies. *J. Phys. Chem. B* **2006**, *110*, 7129−7138.
(37) Antonov, L.; Stoyanov, S. Analysis of the Overlapping Bands in UV-Vis Absorption Spectroscopy. *Appl. Spectrosc.* **1993**, *47*, 1030−1035.
(38) Sarap, C. S.; Adhikari, B.; Meng, S.; Uhlig, F.; Fyta, M. Optical Properties of Single- and Double-Functionalized Small Diamondoids. *J. Phys. Chem. A* **2018**, *122*, 3583−3593.
(39) Hohenberg, P.; Kohn, W. Inhomogeneous Electron Gas. *Phys. Rev.* **1964**, *136*, B864.
(40) Kohn, W.; Sham, L. J. Self-Consistent Equations Including Exchange and Correlation Effects. *Phys. Rev.* **1965**, *140*, A1133.
(41) Zhao, Y.; Truhlar, D. G. Density Functionals with Broad Applicability in Chemistry. *Acc. Chem. Res.* **2008**, *41*, 157−167.
(42) Vovusha, H.; Sanyal, S.; Sanyal, B. Interaction of Nucleobases and Aromatic Amino Acids with Graphene Oxide and Graphene Flakes. *J. Phys. Chem. Lett.* **2013**, *4*, 3710−3718.
(43) Umadevi, D.; Sastry, G. N. Quantum Mechanical Study of Physisorption of Nucleobases on Carbon Materials: Graphene versus Carbon Nanotubes. *J. Phys. Chem. Lett.* **2011**, *2*, 1572−1576.
(44) Schmidt, M. W.; Baldridge, K. K.; Boatz, J. A.; Elbert, S. T.; Gordon, M. S.; Jensen, J. H.; Koseki, S.; Matsunaga, N.; Nguyen, K. A.; Su, S.; Windus, T. L.; Dupuis, M.; Montgomery, J. A. General Atomic and Molecular Electronic Structure System. *J. Comput. Chem.* **1993**, *14*, 1347−1363.
(45) Gordon, M. S.; Schmidt, M. W. In *Theory and Applications of Computational Chemistry*; Dykstra, C. E., Frenking, G., Kim, K. S., Scuseria, G. E., Eds.; Elsevier: Amsterdam, 2005; pp 1167−1189.
(46) Boys, S. F.; Bernardi, F. d. The Calculation of Small Molecular Interactions by the Differences of Separate Total Energies. Some Procedures with Reduced Errors. *Mol. Phys.* **1970**, *19*, 553−566.
(47) Hopffgarten, M. v.; Frenking, G. Energy Decomposition Analysis. *Wiley Interdisciplinary Reviews: Computational Molecular Science* **2012**, *2*, 43−62.
(48) Gross, E. K.; Dreizler, R. M. *Density Functional Theory*; Springer Science & Business Media, 2013; Vol. 337.
(49) Yanai, T.; Tew, D. P.; Handy, N. C. A New Hybrid Exchange-correlation Functional Using the Coulomb-attenuating Method (CAM-B3LYP). *Chem. Phys. Lett.* **2004**, *393*, 51−57.
(50) Govind, N.; Valiev, M.; Jensen, L.; Kowalski, K. Excitation Energies of Zinc Porphyrin in Aqueous Solution using Long-range Corrected Time-dependent Density Functional Theory. *J. Phys. Chem. A* **2009**, *113*, 6041−6043.
(51) Jensen, L.; Govind, N. Excited States of DNA Base Pairs using Long-range Corrected Time-dependent Density Functional Theory. *J. Phys. Chem. A* **2009**, *113*, 9761−9765.
(52) Baer, R.; Livshits, E.; Salzner, U. Tuned Range-separated Hybrids in Density Functional Theory. *Annu. Rev. Phys. Chem.* **2010**, *61*, 85−109.
(53) Lopata, K.; Govind, N. Modeling Fast Electron Dynamics with Real-time Time-Dependent Density Functional Theory: Application to Small Molecules and Chromophores. *J. Chem. Theory Comput.* **2011**, *7*, 1344−1355.
(54) Dreuw, A.; Plötner, J.; Wormit, M.; Head-Gordon, M.; Dutoi, A. D. An Additive Long-Range Potential to Correct for the Charge-Transfer Failure of Time-dependent Density Functional Theory. *Z. Phys. Chem.* **2010**, *224*, 311−324.
(55) Valiev, M.; Bylaska, E. J.; Govind, N.; Kowalski, K.; Straatsma, T. P.; Van Dam, H. J.; Wang, D.; Nieplocha, J.; Apra, E.; Windus, T. L. NWChem: A Comprehensive and Scalable Open-source Solution for Large Scale Molecular Simulations. *Comput. Phys. Commun.* **2010**, *181*, 1477−1489.
(56) Partovi-Azar, P.; Kaghazchi, P. Time-dependent Density Functional Theory Study on Direction-dependent Electron and Hole Transfer Processes in Molecular Systems. *J. Comput. Chem.* **2017**, *38*, 698−703.
(57) Tassi, M.; Morphis, A.; Lambropoulos, K.; Simserides, C. RT-TDDFT Study of Hole Oscillations in B-DNA Monomers and Dimers. *Cogent Physics* **2017**, *4*, 1361077.
(58) Eichkorn, K.; Treutler, O.; Öhm, H.; Häser, M.; Ahlrichs, R. Auxiliary Basis Sets to Approximate Coulomb Potentials. *Chem. Phys. Lett.* **1995**, *240*, 283−290.
(59) Kaduk, B.; Kowalczyk, T.; Van Voorhis, T. Constrained Density Functional Theory. *Chem. Rev.* **2012**, *112*, 321−370.

DOI: 10.1021/acsabm.8b00011
ACS Appl. Bio Mater. 2018, 1, 59−69